Negative Results Vol. 4, No. 5 / 15 May 2021 / OSA Continuum 1452
OSA CONTINUUM

# Hyperfine structure of molecular iodine measured using a light source with a laser linewidth at the megahertz level

KAZUMICHI YOSHII,[1,2,3] CHAOYUN CHEN,[1] HARUKI SAKAGAMI,[1] AND FENG-LEI HONG[1,4]

[1]*Department of Physics, Graduate School of Engineering Science, Yokohama National University, Yokohama, Kanagawa 240-8501, Japan*
[2]*Present address: Institute of Post-LED Photonics, Tokushima University, 2-1 Minami-Josanjima, Tokushima, Tokushima 770-8506, Japan*
[3]*yoshii.kazumichi@tokushima-u.ac.jp*
[4]*hong-feng-lei-mt@ynu.ac.jp*

**Abstract:** The hyperfine structure of the absorption lines of molecular iodine at 531 nm was measured using a low-cost, coin-sized light source with a laser linewidth at the megahertz level. The measured hyperfine splittings were found to be systematically smaller than those measured using a narrow-linewidth diode laser. The theoretical fit of the measured hyperfine splittings to a four-term Hamiltonian, including the electric quadrupole, spin-rotation, tensor spin-spin, and scalar spin-spin interactions, does not clarify the observed systematic deviation in the measurement, but instead results in deviated hyperfine constants from reliable literature values beyond the uncertainties. Therefore, the theoretical fit, which is usually used to validate the measurement, does not provide the validation function in the case of megahertz level laser linewidths.



## 1. Introduction

Laser spectroscopy and frequency stabilization are of significant interest in a wide range of applications, including fundamental science and technologies that support precision measurement and broadband communication networks [1]. Frequency-stabilized lasers based on molecular iodine ($^{127}I_2$) are used in length measurement [2,3], gravitational wave detection [4–6], and studies on atomic and molecular physics. Several lasers, which are stabilized to hyperfine components of the rovibrational transitions of $^{127}I_2$, are recommended as frequency and length standards by the International Committee for Weights and Measures (CIPM) [1,7]. In addition, iodine-stabilized lasers are used as flywheel oscillators and absolute frequency markers for optical frequency combs [8,9].

As iodine-stabilized lasers rely on the hyperfine components of iodine transitions, the hyperfine structure of $^{127}I_2$ is an important topic in high-resolution spectroscopy and laser frequency stabilization. In molecular physics, the results of high-resolution spectroscopy have reduced the deviation from the theoretical fit of hyperfine structures, and hence, increased the accuracy of the hyperfine constants [10]. Meanwhile, the theoretical fit of hyperfine components is used to verify the reliability of iodine-stabilized lasers. To understand the hyperfine structure of $^{127}I_2$ across a wide range of spectra, hyperfine constants have been used to derive empirical formulae that describe the dependence of the hyperfine structure on vibrational and rotational quantum numbers [11]. The precise measurement of hyperfine structures at different wavelengths enables us to obtain a better understanding of the structure's vibrational and rotational characteristics and improve the empirical formulae.

#420628 https://doi.org/10.1364/OSAC.420628
Journal © 2021 Received 26 Jan 2021; revised 2 Apr 2021; accepted 5 Apr 2021; published 26 Apr 2021

OSA CONTINUUM

Precision spectroscopy of $^{127}I_2$ and frequency stabilization was performed using different types of laser sources. The 633-nm iodine-stabilized He–Ne laser is the most popular iodine-stabilized laser for length applications. Using high-resolution laser spectroscopy, iodine-stabilized Nd:YAG lasers based on strong 532-nm absorption lines were developed with excellent laser frequency stability [12–14]. Except for the He–Ne (linewidth ~ 10 kHz) and Nd:YAG (linewidth ~ kHz) lasers, external-cavity diode lasers (ECDLs; linewidth ~ 100 kHz) have also been used to measure hyperfine structures of $^{127}I_2$ [15]. Unlike the usual ECDLs, a planar-waveguide ECDL (PWECDL) at 1064 nm has a linewidth of several kHz, and has been used for laser frequency stabilization and measurement [16,17]. Recently, an ultracompact iodine-stabilized laser was developed based on Doppler-free spectroscopy using a low-cost, coin-sized laser (CSL) source (linewidth ~ MHz) at 531 nm [18]. Such CSLs have also been used for the demonstration of high-resolution spectroscopy of $^{127}I_2$ [19]. However, the hyperfine structure of iodine lines has not been measured using CSLs. Since CSLs cover wide frequency ranges at 531 nm, 561 nm and 594 nm [19] and are significantly low cost, CSLs could be useful light sources for the study of iodine hyperfine constants in these undeveloped wavelength regions. Furthermore, the measurement and theoretical fit of hyperfine structures should provide useful information on the reliability of such low-cost iodine-stabilized lasers, which may be commercialized or built in other precision measuring equipment.

Thus, we measured the hyperfine structures of $^{127}I_2$ using a coin-sized light source in this study. The hyperfine constants were obtained by fitting the measured hyperfine structures to a four-term Hamiltonian [10]. Unfortunately, we found that the measured hyperfine structures and obtained hyperfine constants systematically deviated from those obtained using a narrow-linewidth laser [17]. Thus, the theoretical fit cannot be used to determine the iodine hyperfine constants in the undeveloped wavelength regions covered by the CSLs. More importantly, the theoretical fit does not provide useful information on the reliability of the measurement and the low-cost iodine-stabilized lasers based on CSLs.

## 2. Experimental setup and results

A CSL module (QDLaser, QLD0593-3220) was used as the light source. The laser module comprises a distributed-feedback (DFB) diode laser operating at 1063 nm, semiconductor optical amplifier, and periodically poled lithium niobate crystal for second harmonic generation (SHG) at 531 nm. The laser linewidth of the fundamental light was ~1 MHz [19]. In the spectroscopy part, the SHG laser light was transmitted to an iodine spectrometer based on saturation spectroscopy using the modulation transfer technique [20,21]. The observed sub-Doppler hyperfine structures of $^{127}I_2$ were used for laser frequency stabilization. To measure the hyperfine structures, the fundamental DFB laser light was sent to an optical frequency comb system for frequency measurement. A more detailed experimental setup and their parameters are provided in Ref. [19].

From the available absorption lines within the tuning range of the coin-sized laser module [19], we selected and studied 6 lines: P(32)32-0, P(33)32-0, P(35)32-0, R(35)32-0, R(36)32-0, and R(41)32-0 transitions, which are relatively strong and have the same upper state vibrational quantum number $v' = 32$. Figures 1(a) and 1(b) show the observed modulation transfer signals of the R(36)32-0 and P(35)32-0 transitions, respectively, obtained using the CSL. Laser frequency scanning was performed by tuning the injection current of the laser. The powers of the pump and probe beams were 5.2 and 0.14 mW for the R(36)32-0 transition and 4.8 and 0.12 mW for the P(35)32-0 transition, respectively. The diameters of the pump and probe beams were 1.4 mm and 1.3 mm, respectively. The cold-finger temperature of the iodine cell was held at 0 °C, corresponding to an iodine pressure of 4.0 Pa. The temperature of the cell body matched the controlled room temperature of 23 °C. For even (odd) $J$ numbers of the ground rotational states, the rovibrational energy level is split into 15 (21) sublevels, resulting in 15 (21) hyperfine

OSA CONTINUUM

components. The signal-to-noise ratio (S/N) of the $a_1$ component of the R(36)32-0 transition was approximately 173 for a bandwidth of 100 Hz. The S/N of the $a_3$ component of the P(35)32-0 transition was approximately 73 for a bandwidth of 1 kHz. The spectral linewidths of these components were 5-6 MHz. The asymmetric spectral line shapes observed for the hyperfine components are partly due to the laser frequency jitter. Meanwhile, there should be also contributions from the reason discussed in Section 3. For comparison, in Fig. 1(c), we also show the modulation transfer signals of the P(35)32-0 line observed using a PWECDL with a linewidth of several kHz [17]. The S/N of the $a_3$ component of the P(35)32-0 transition was approximately 560 for a bandwidth of 30 Hz. The spectral linewidth was 1.6 MHz. In this case, the laser frequency scanning was performed by tuning the temperature of the PWECDL. The scanned spectra in Figs. 1(b) and 1(c) show slightly different hyperfine splittings due to the different nonlinearities of the frequency scan in the two cases.

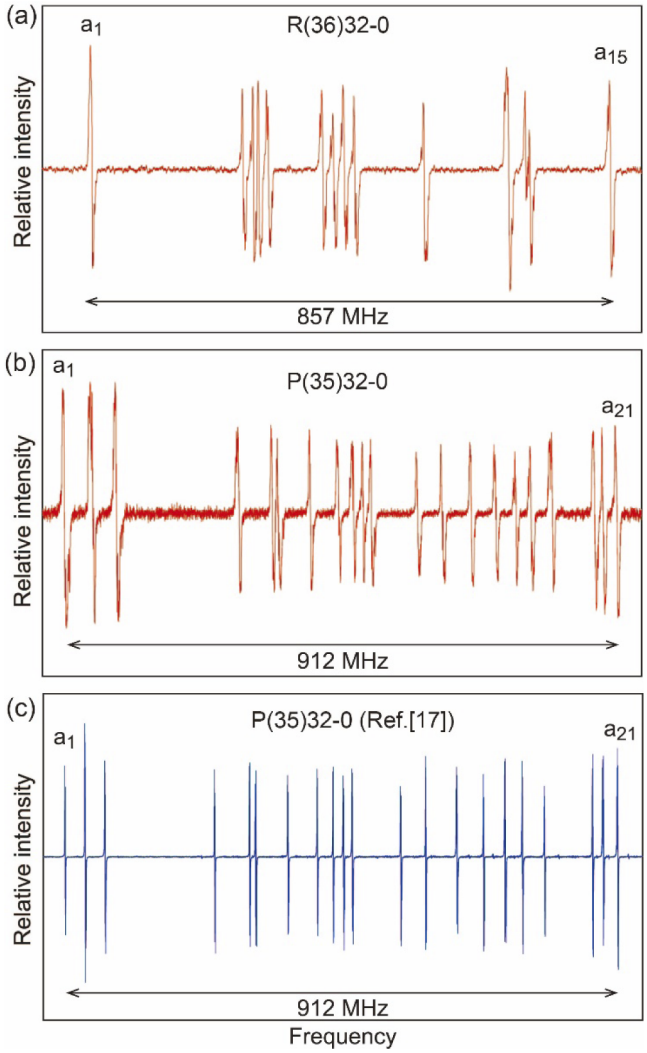


**Fig. 1.** Doppler-free spectra of (a) the R(36)32-0 transition of molecular iodine obtained over a bandwidth of 100 Hz, (b) the P(35)32-0 transition of molecular iodine obtained over a bandwidth of 1 kHz, and (c) the P(35)32-0 transition of molecular iodine obtained over a bandwidth of 30 Hz using the planar-waveguide external-cavity diode laser [17].

OSA CONTINUUM

Several systematic frequency shifts and uncertainties of the iodine-stabilized CSL locked on the $a_1$ component of R(36)32-0 transition were investigated. Figure 2(a) shows the measured frequency shift of the CSL as a function of the pump power. The measured slope of the pump power shift was −0.40 kHz/mW. The uncertainty in the determination of the laser power was estimated to be < 10%. This gives rise to a frequency uncertainty of < 0.26 kHz. Figure 2(b) shows the measured pressure shift of the CSL. The measured slope of the pressure shift was −2.1 kHz/Pa. The uncertainty in the determination of the solid-state iodine inside the cell cold-finger was estimated to be < 0.5 K. This corresponds to a pressure uncertainty of < 0.2 Pa, resulting in a frequency uncertainty of < 0.4 kHz. Figure 2(c) shows the measured frequency shift caused by the servo electronic offset. The slope of this effect was −8.1 kHz/mV. We adjusted the servo electric offset to less than 0.5 mV, which results in a frequency uncertainty of < 4 kHz. Figure 2(d) and 2(e) show the measured frequency shifts caused by the misalignment of the pump and probe beams [14]. The measured slope of this shift for vertical direction and that for horizontal direction were 15 kHz/mrad and 5.2 kHz/mrad, respectively. The uncertainty of the pointing direction of the pump beam was estimated to be < 0.1 mrad. This gives rise to a frequency uncertainties of < 2 kHz for vertical and < 0.5 kHz for horizontal, respectively. The most significant contributions to the estimated frequency uncertainty of the iodine-stabilized CSL are summarized in Table 1. Contamination in the iodine cell causes a frequency shift. This effect can add an uncertainty of 5 kHz to the measurement results [14]. The uncertainty of the frequency reference used in the frequency comb is the repeatability (1.5 kHz) of the iodine-stabilized Nd:YAG laser [16]. Figure 2(f) shows the results of 13 measurements for the $a_1$ component of the R(36)32-0 transition obtained over several days. Each measurement shown in Fig. 2(f) was calculated from more than 2000 beat frequency data, where each frequency datum was measured by the frequency counter with a gate time of 1 s. The uncertainty bar in this figure was given by the Allan standard deviation at the longest averaging time. The average of the thirteen measured frequencies in Fig. 2(f) was 564 074 632 658 kHz. The statistical uncertainty (7.2 kHz) is calculated by the standard deviation of the thirteen measurements. The total uncertainty was estimated to be 9.9 kHz (relatively $1.8 \times 10^{-11}$), including the statistical uncertainty of 7.2 kHz.

**Table 1. Most significant contributions to the estimated frequency uncertainty of a CSL locked on the $a_1$ component of the R(36)32-0 transition**

| Effect | Sensitivity | Uncertainty |
|---|---|---|
| Power shift | –0.40 kHz/mW | < 0.26 kHz |
| Pressure shift | –2.1 kHz/Pa | < 0.4 kHz |
| Servo electronics offset | –8.1 kHz/mV | < 4 kHz |
| Alignment of the pump and probe beams | 15 kHz/mrad | < 2 kHz |
| –vertical | | |
| –horizontal | 5.2 kHz/mrad | < 0.5 kHz |
| Cell impurity | — | 5 kHz |
| Frequency reference of the comb | — | 1.5 kHz |
| Statistics | | 7.2 kHz |
| Total uncertainty | — | 9.9 kHz |
| Relative uncertainty | — | $1.8\times10^{-11}$ |

To determine the iodine hyperfine splittings, an absolute frequency measurement was applied to each component. The iodine-stabilized CSL was locked in succession to all 15 or 21 hyperfine components. As an example, Table 2 shows the measured hyperfine splittings of the P(35)32-0 transition obtained from the calculation of the frequency difference between each component and

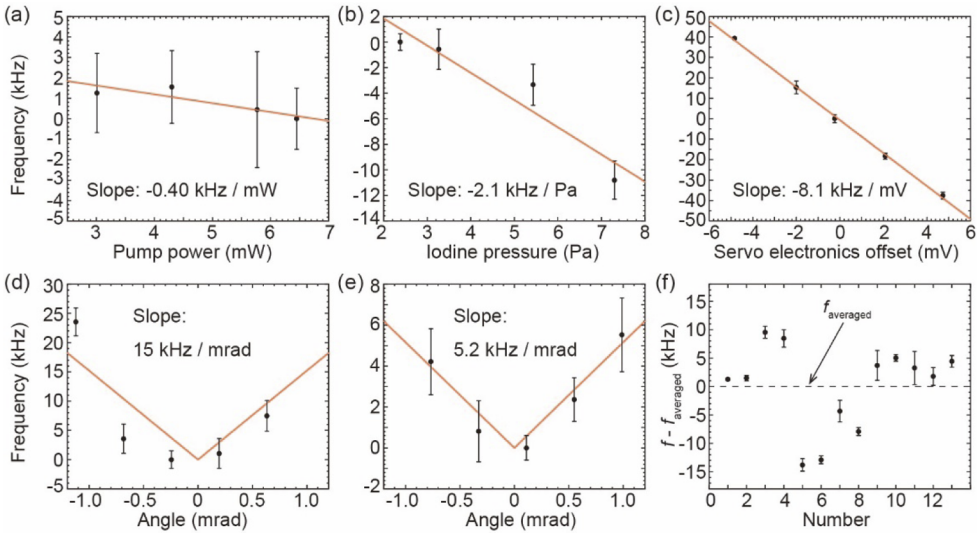


**Fig. 2.** Measured frequency shift of the coin-sized laser locked to the $a_1$ component of the R(36)32-0 transition: (a) power shift, (b) pressure shift, (c) shift due to the servo electrical offset, shift due to the misalignment of the pump and probe beams for (d) vertical direction, and that for (e) horizontal direction. The solid red line in each figure shows the best fit of a linear function using the least square method. (f) The repeatability of the frequency measurement of the $a_1$ component of the R(36)32-0 transition. The dashed line indicates the average of the thirteen measured frequencies. The standard deviation is 7.2 kHz.

the first $a_1$ component. The measurement uncertainty of the hyperfine splittings is limited by the repeatability of the iodine-stabilized CSL at approximately 10 kHz.

The hyperfine interactions of $^{127}I_2$ can be described by an effective Hamiltonian, including the electric quadrupole, spin-rotation, tensor spin-spin, and scalar spin-spin interactions; $eQq$, $C$, $d$, and $\delta$, respectively, are the corresponding hyperfine constants for each of these interactions. We calculated the eigenstates of the Hamiltonian based on the procedure described by Bordé *et al.* [10]. By theoretically fitting the observed hyperfine splittings, accurate values can be obtained for the differences in the hyperfine constants between the upper and lower states ($\Delta eQq$, $\Delta C$, $\Delta d$, and $\Delta\delta$); however, only rough estimates can be made of the absolute values for the respective states. In the present calculation, the hyperfine splittings were fitted to the measured values by a nonlinear least-squares fit [20], with varying upper-state hyperfine constants ($eQq'$, $C'$, $d'$, and $\delta'$). The lower state $eQq''$ was calculated from Ref. [21], while $C''$, $d''$, and $\delta''$ were fixed at 3.154, 1.524, and 3.705 kHz, respectively [22]. The calculated hyperfine splittings of the P(35)32-0 transition are also listed in Table 2. The standard deviation (SD) of the theoretical fit was calculated from (Obs.-Cal.), and found to be 16 kHz, which is limited by the measurement uncertainty of the hyperfine splittings. Table 3 shows the fitted hyperfine constants for the P(35)32-0 transition and the 5 other transitions studied herein. The SDs of the theoretical fits for the P(32)32-0, P(33)32-0, R(35)32-0, R(36)32-0, and R(41)32-0 transitions were 14, 16, 25, 18, and 14 kHz, respectively. Meanwhile, the uncertainties of the main hyperfine constant $\Delta eQq$ for the transitions ranged from 10 to 30 kHz.

The hyperfine structure of the P(35)32-0 transition was also studied using the PWECDL [17] (as shown in Fig. 1(c)). For comparison, the observed and calculated hyperfine splittings obtained in Ref. [17] are listed in Table 2. The SD of the theoretical fit for the PWECDL case is 1.4 kHz, approximately one order of magnitude smaller than that for the current CSL case. Figure 3 shows the frequency difference of the hyperfine splittings in: (1) $f_{obs} - f_{cal}$ for the CSL case; (2) $f_{obs} - f_{cal}$

OSA CONTINUUM

**Table 2. Observed and calculated hyperfine splittings of the P(35)32-0 transition[a]**

| | CSL | | PWECDL [17] | |
|---|---|---|---|---|
| | Obs. | Cal. | Obs. | Cal. |
| $a_1$ | 0 | 19 | 0.0 | -0.8 |
| $a_2$ | 37,058 | 37,080 | 37,056.2 | 37,055.9 |
| $a_3$ | 71,373 | 71,382 | 71,354.5 | 71,355.3 |
| $a_4$ | 259,870 | 259,842 | 259,842.7 | 259,842.3 |
| $a_5$ | 317,429 | 317,398 | 317,390.7 | 317,390.5 |
| $a_6$ | 328,214 | 328,228 | 328,222.4 | 328,222.7 |
| $a_7$ | 382,155 | 382,150 | 382,149.4 | 382,149.3 |
| $a_8$ | 430,479 | 430,488 | 430,493.5 | 430,495.3 |
| $a_9$ | 456,310 | 456,291 | 456,295.6 | 456,296.0 |
| $a_{10}$ | 472,784 | 472,781 | 472,779.8 | 472,781.9 |
| $a_{11}$ | 488,287 | 488,288 | 488,285.0 | 488,285.3 |
| $a_{12}$ | 566,667 | 566,654 | 566,663.5 | 566,662.2 |
| $a_{13}$ | 608,006 | 607,996 | 608,008.3 | 608,007.5 |
| $a_{14}$ | 657,453 | 657,445 | 657,460.7 | 657,459.7 |
| $a_{15}$ | 699,551 | 699,556 | 699,582.0 | 699,582.9 |
| $a_{16}$ | 734,573 | 734,571 | 734,595.3 | 734,593.6 |
| $a_{17}$ | 762,464 | 762,464 | 762,483.7 | 762,481.7 |
| $a_{18}$ | 797,357 | 797,354 | 797,386.3 | 797,385.1 |
| $a_{19}$ | 873,872 | 873,887 | 873,909.2 | 873,912.4 |
| $a_{20}$ | 889,671 | 889,684 | 889,721.5 | 889,722.7 |
| $a_{21}$ | 912,223 | 912,236 | 912,267.3 | 912,266.5 |
| SD | | 16 | | 1.4 |

[a]All values are in kHz. SD is the standard deviation of the fit.

**Table 3. Fitted hyperfine constants**

| | $\Delta eQq$ (MHz) | $\Delta C$ (kHz) | $\Delta d$ (kHz) | $\Delta\delta$ (kHz) |
|---|---|---|---|---|
| P(32)32-0 | 1,908.27(3) | 85.01(5) | -42(1) | -11(1) |
| P(33)32-0 | 1,908.24(1) | 85.11(2) | -44.4(6) | -10.5(4) |
| P(35)32-0 | 1,908.32(2) | 85.23(3) | -42(1) | -12(1) |
| P(35)32-0[a] | 1,908.445(2) | 85.208(3) | -43.77(3) | -10.60(1) |
| R(35)32-0 | 1,908.19(3) | 85.23(5) | -49.2 (4) | -9(1) |
| R(36)32-0 | 1,908.16(3) | 85.29(3) | -43.7(7) | -9.1(9) |
| R(41)32-0 | 1,908.21(1) | 85.52(2) | -44(1) | -11.9(6) |

[a]Reference [17]

OSA CONTINUUM

for the PWECDL case; (3) $f_{\mathrm{CSL}}-f_{\mathrm{PWECDL}}$ for the observation case; and (4) $f_{\mathrm{CSL}}-f_{\mathrm{PWECDL}}$ for the calculation case. The residual ($f_{\mathrm{obs}}-f_{\mathrm{cal}}$) for the CSL case is larger than that for the PWECDL case, as can be understood from the difference of the SDs of the theoretical fit in the two cases. However, both residuals are around zero frequency. Meanwhile, the frequency difference of the hyperfine splittings ($f_{\mathrm{CSL}}-f_{\mathrm{PWECDL}}$) for both the observation and calculation cases approaches a considerably negative value when the number of hyperfine components increases. This indicates that the hyperfine splittings observed using the CSL are smaller than those observed using the PWECDL. However, the theoretical fit can also reproduce the results observed using the CSL.

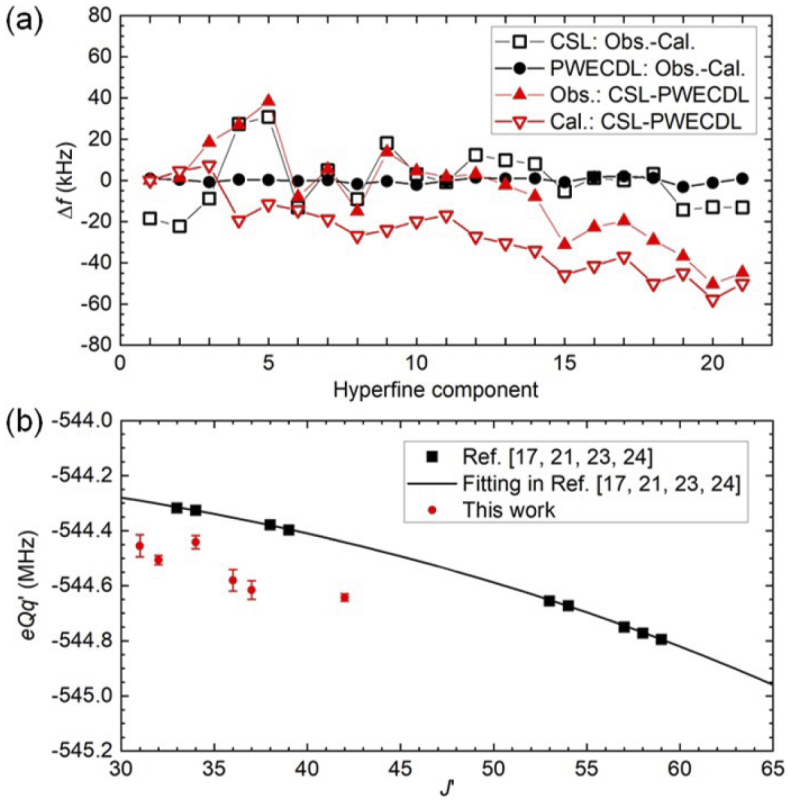


**Fig. 3.** (a) Frequency difference of the hyperfine splittings. Frequency values of the planar-waveguide external-cavity diode laser case were taken from Ref. [17]. (b) Rotation dependence of the upper state hyperfine constant $eQq'$ for the $v'=32$ case. Literature values were taken from Ref. [17,21,23,24].

The hyperfine constants of the P(35)32-0 transition obtained in the PWECDL case [17] are also listed in Table 3. We found that $\Delta eQq$ is the main hyperfine constant contributing to the difference in the two cases, while the other hyperfine constants remained approximately the same. For upper states $v'=32$, the hyperfine constant $eQq'$ can be expressed as a function of the rotational quantum number $J'$ (shown in Fig. 3(b) by the solid curve) [17]. Using the formula of the lower state $eQq''$ [21], we calculated $eQq'$ for the transitions studied in the present experiment, which are shown as solid circles in Fig. 3(b). For comparison, $eQq'$ of the transitions studied in previous publications [17,21,23,24] are also shown in Fig. 3(b) as solid squares (uncertainties are small and not seen on this scale). Consequently, the hyperfine constants $eQq'$ obtained in the present experiment are all smaller than those obtained in previous studies. Therefore, the hyperfine structures of the transitions, which were observed using the CSL, have shrunk. We

OSA CONTINUUM

note that the dispersion of the $eQq'$ values obtained in the present experiment is mainly due to the measurement uncertainties of the hyperfine structure using the CSL.

## 3. Discussion and conclusion

Here, we discuss the reason for the shrinking of the hyperfine structures in the observation using the CSL. When lasers with relatively large linewidths are used, spectroscopy is usually performed with relatively large gas pressure and laser power, resulting in a relatively large spectral linewidth; otherwise, the spectral linewidth is usually split, owing to the frequency jitter of the laser. With the high gas pressure, the background linear absorption (shown as a solid curve in Fig. 4) was relatively large in the present experiment. In saturation spectroscopy using the modulation transfer technique, the S/N depends on the modulation frequency [25]. To achieve a high S/N, we needed to set a relatively large modulation frequency of 800 kHz [19]. When the modulation frequency is large, in the observation of the first-half hyperfine components of the P(35)32-0 line ($a_1$ to $a_{10}$), the +1 order sideband at higher frequency experiences larger absorption compared to the −1 order sideband (shown in Fig. 4). This results in an offset of the line center in the observed spectrum at the low-frequency side, as well as an asymmetric line shape (for example, the spectrum of the $a_3$ component shown in Fig. 4). The frequency lock using the electrical zero voltage will eventually result in the laser being locked at the high-frequency side. Whereas, in the observation of the last half of the hyperfine components ($a_{11}$ to $a_{21}$), the laser will be locked at the low-frequency side. Therefore, the hyperfine structure shrinks under the experimental conditions of large modulation frequency and linear absorption, which are used when the laser linewidth is relatively large. We note here that the red and blue spots in Fig. 4 indicating the offset of the line center and the lock point, respectively, are images for the explanation of the problem we are facing. The observed asymmetric spectral line shapes are due to not only the relatively large laser linewidth discussed here, but also the laser frequency jitter during the frequency scan. Therefore, quantitative estimation from the line shape is not easy in the case. Furthermore, the frequency jitter in the horizontal axis is also transferred to the intensity noise in the vertical axis through the line shape. This again makes quantitative estimation more difficult.

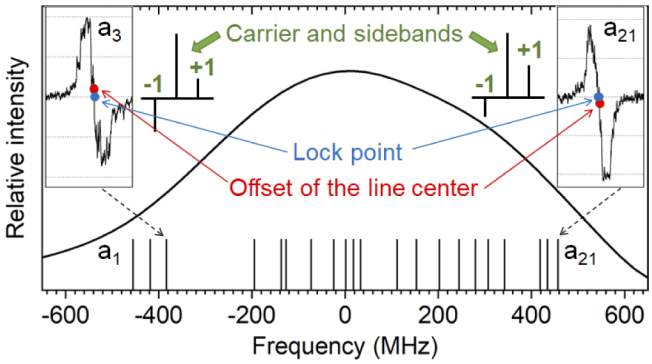


**Fig. 4.** Background linear absorption and its influence on Doppler-free modulation spectroscopy.

In conclusion, we found that the measured hyperfine splittings, using a coin-sized light source with a laser linewidth at the megahertz level, are systematically smaller than those measured using a narrow-linewidth diode laser. However, the theoretical fit does not clarify the correctness of the measurements, and results in incorrect hyperfine constants of the electric quadrupole interaction ($\Delta eQq$).

**Funding.** Japan Society for the Promotion of Science (KAKENHI 18H01898, KAKENHI 18H03886).

OSA CONTINUUM

**Acknowledgments.** We are grateful to J. Nomura and K. Ikeda for their technical assistance in the experiment, and T. Kobayashi for the helpful discussions on the fitting calculation.

**Disclosures.** The authors declare no conflicts of interest related to this article.

## References

1. F.-L. Hong, "Optical frequency standards for time and length applications," Meas. Sci. Technol. **28**(1), 012002 (2017).
2. Y. Bitou, K. Sasaki, S. Iwasaki, and F.-L. Hong, "Compact $I_2$-stabilized frequency-doubled Nd:YAG laser for long gauge block interferometer," Jpn. J. Appl. Phys. **42**(Part 1, No. 5A), 2867–2871 (2003).
3. Y. Bitou, T. Kobayashi, and F.-L. Hong, "Compact and inexpensive iodine-stabilized diode laser system with an output at 531 nm for gauge block interferometers," Precis. Eng. **47**, 528–531 (2017).
4. M. Musha, T. Kanaya, K. Nakagawa, and K. Ueda, "The short- and long-term frequency stabilization of an injection-locked Nd:YAG laser in reference to a Fabry-Perot cavity and an iodine saturated absorption line," Opt. Commun. **183**(1-4), 165–173 (2000).
5. W. Kokuyama, K. Numata, and J. Camp, "Simple iodine reference at 1064 nm for absolute laser frequency determination in space applications," Appl. Opt. **49**(32), 6264–6267 (2010).
6. B. Argence, H. Halloin, O. Jeannin, P. Prat, O. Turazza, E. de Vismes, G. Auger, and E. Plagnol, "Molecular laser stabilization at low frequencies for the LISA mission," Phys. Rev. D **81**(8), 082002 (2010).
7. F. Riehle, P. Gill, F. Arias, and L. Robertsson, "The CIPM list of recommended frequency standard values: Guidelines and procedures," Metrologia **55**(2), 188–200 (2018).
8. J. Ye, L.-S. Ma, and J. L. Hall, "Molecular iodine clock," Phys. Rev. Lett. **87**(27), 270801 (2001).
9. F.-L. Hong, M. Takamoto, R. Higashi, Y. Fukuyama, J. Jiang, and H. Katori, "Frequency measurement of a Sr lattice clock using an SI-second-referenced optical frequency comb linked by a global positioning system (GPS)," Opt. Express **13**(14), 5253–5262 (2005).
10. C. J. Bordé, G. Camy, B. Decomps, J.-P. Descoubes, and J. Vigué, "High precision saturation spectroscopy of $^{127}I_2$ with argon lasers at 5145 Å and 5017 Å. I. Main resonances," J. Phys. (Paris) **42**(10), 1393–1411 (1981).
11. A. Razet and S. Picard, "A test of new empirical formulas for the prediction of hyperfine component frequencies in $^{127}I_2$," Metrologia **34**(2), 181–186 (1997).
12. A. Arie, S. Schiller, E. K. Gustafson, and R. L. Byer, "Absolute frequency stabilization of diode-laser-pumped Nd:YAG lasers to hyperfine transitions in molecular iodine," Opt. Lett. **17**(17), 1204–1206 (1992).
13. J. L. Hall, L.-S. Ma, M. Taubman, B. Tiemann, F.-L. Hong, O. Pfister, and J. Ye, "Stabilization and frequency measurement of the $I_2$-stabilized Nd:YAG laser," IEEE Trans. Instrum. Meas. **48**(2), 583–586 (1999).
14. F.-L. Hong, J. Ishikawa, Y. Zhang, R. Guo, A. Onae, and H. Matsumoto, "Frequency reproducibility of an iodine-stabilized Nd: YAG laser at 532 nm," Opt. Commun. **235**(4-6), 377–385 (2004).
15. F. Cheng, K. Deng, K. Liu, H. Liu, J. Zhang, and Z. Lu, "Absolute frequency measurement of molecular iodine hyperfine transitions at 534 nm," J. Opt. Soc. Am. B **36**(7), 1816–1822 (2019).
16. K. Yoshii, H. Sakagami, H. Yamamoto, S. Okubo, H. Inaba, and F.-L. Hong, "High-resolution spectroscopy and laser frequency stabilization using a narrow-linewidth planar-waveguide external cavity diode laser at 1063 nm," Opt. Lett. **45**(1), 129–132 (2020).
17. H. Sakagami, K. Yoshii, T. Kobayashi, and F.-L. Hong, "Absolute frequency and hyperfine structure of $^{127}I_2$ transitions at 531.5 nm by precision spectroscopy using a narrow-linewidth diode laser," J. Opt. Soc. Am. B **37**(4), 1027–1034 (2020).
18. T. Kobayashi, D. Akamatsu, K. Hosaka, H. Inaba, S. Okubo, T. Tanabe, M. Yasuda, A. Onae, and F.-L. Hong, "Compact iodine-stabilized laser operating at 531 nm with stability at the $10^{-12}$ level and using a coin-sized laser module," Opt. Express **23**(16), 20749–20759 (2015).
19. J. Nomura, K. Yoshii, Y. Hisai, and F.-L. Hong, "Precision spectroscopy and frequency stabilization using coin-sized laser modules," J. Opt. Soc. Am. B **36**(3), 631–637 (2019).
20. T. Kobayashi, D. Akamatsu, K. Hosaka, H. Inaba, S. Okubo, T. Tanabe, M. Yasuda, A. Onae, and F.-L. Hong, "Absolute frequency measurements and hyperfine structures of the molecular iodine transitions at 578 nm," J. Opt. Soc. Am. B **33**(4), 725–734 (2016).
21. F.-L. Hong, J. Ye, L.-S. Ma, S. Picard, C. J. Bordé, and J. L. Hall, "Rotation dependence of electric quadrupole hyperfine interaction in the ground state of molecular iodine by high-resolution laser spectroscopy," J. Opt. Soc. Am. B **18**(3), 379–387 (2001).
22. B. Bodermann, H. Knöckel, and E. Tiemann, "Widely usable interpolation formulae for hyperfine splittings in the $^{127}I_2$ spectrum," Eur. Phys. J. D **19**(1), 31–44 (2002).
23. J. Ye, L. Robertsson, S. Picard, L.-S. Ma, and J. L. Hall, "Absolute frequency atlas of molecular $I_2$ lines at 532 nm," IEEE Trans. Instrum. Meas. **48**(2), 544–549 (1999).
24. F.-L. Hong, J. Ishikawa, A. Onae, and H. Matsumoto, "Rotation dependence of the excited-state electric quadrupole hyperfine interaction by high-resolution laser spectroscopy of $^{127}I_2$," J. Opt. Soc. Am. B **18**(10), 1416–1422 (2001).
25. L.-S. Ma and J. L. Hall, "Optical heterodyne spectroscopy enhanced by an external optical cavity: toward improved working standards," IEEE J. Quantum. Electron. **26**(11), 2006–2012 (1990).